Geoderma 457 (2025) 117290

Contents lists available at ScienceDirect

Geoderma

journal homepage: www.elsevier.com/locate/geoderma

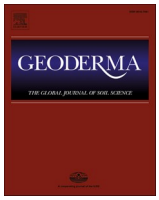

Soil structural indicators as predictors of biological activity under various soil management practices

Frederic Leuther [a,b,1,*], Dorte Fischer [a,c], Naoise Nunan [a,d,2], Katharina H.E. Meurer [a,3], Anke M. Herrmann [a,4]

[a] Department of Soil and Environment, Swedish University of Agricultural Sciences, Uppsala, Sweden
[b] Chair of Soil Physics, University of Bayreuth, Bayreuth, Germany
[c] Marine Environmental Science, Carl von Ossietzky University, Oldenburg, Germany
[d] Institute of Ecology and Environmental Sciences - Paris, Sorbonne Université, CNRS, IRD, INRAe, UPEC, Paris, France

ARTICLE INFO

Handling Editor: Yvan Capowiez

Keywords:
Crop rotation
Tillage regime
Soil structure
Biological activity
Micro-habitat
Calorimetry
X-ray CT

ABSTRACT

Soil structure is a key feature in controlling the turnover of organic matter in soils. The spatial arrangement of solids and pores in agricultural topsoil can be actively influenced by management practices, such as tillage and cropping systems, which in turn can affect the resident microbial communities and their activities. However, carbon mineralisation and microbial activity are usually measured in sieved samples, which provides information on gross potentials under optimal conditions. Under these conditions, the spatial heterogeneities that are specific to different management practices are reduced or totally removed. In this study, we combined X-ray computer tomography (X-ray CT) and isothermal calorimetry to investigate the effect of soil structure on heat dissipation, as an indicator of biological activity. Samples were collected from the topsoil of a long-term field experiment (12 years) that included four different land uses: conventional *vs.* reduced tillage, each with either maize or winter wheat as the main crop in the rotation. We compared the response of undisturbed soil cores (3 cm in height, 2.7 cm in diameter) to the addition of water and glucose in specific pore sizes, ranging in radii of 15 to 75 μm or 3 to 75 μm. The pore structure and indicators of particulate organic material were quantified using X-ray CT with a voxel resolution of 15 μm. This allowed us to distinguish between the effects of crop rotation and tillage regime on biological activity, soil structure and the feedback between the two. Heat dissipation correlated significantly with X-ray CT derived porosity, pore surface density and soil matrix grey value, all of which were affected by both tillage regime and crop rotation. Heat dissipation in maize plots after glucose addition to the pore size range with radii of 3 to 75 μm was greater than in the winter wheat systems, but not when added to the pore size range with radii of 15 to 75 μm. The study showed that structural indicators can explain up to 81 % and 95 % of the variance in total heat dissipation after glucose and water addition, respectively, but only 60 % of the heat dynamics, here defined as the time taken for 50 % of total heat to be dissipated. The results emphasise the importance of soil structure in regulating microbial decomposition of soil organic matter and warrants further investigations.

1. Introduction

Soil is a major reservoir of carbon (C), and soil management practices can influence whether soils act as sinks or sources for atmospheric carbon dioxide (CO_2). For instance, field-scale management practices can affect C and nutrient cycling due to the creation of micro-scale heterogeneities (Hartmann and Six 2023). The balance between microbial decomposition of organic matter (OM) and protection of C within the soil structure determines whether soils can be considered as C sinks or sources (Lehmann et al. 2020). Understanding the mechanisms and

* Corresponding author.
E-mail address: frederic.leuther@uni-bayreuth.de (F. Leuther).
[1] https://orcid.org/0000-0001-6955-7892.
[2] https://orcid.org/0000-0003-3448-7171.
[3] https://orcid.org/0000-0002-8880-9650.
[4] https://orcid.org/0000-0002-6273-1234.

https://doi.org/10.1016/j.geoderma.2025.117290
Received 4 November 2024; Received in revised form 2 April 2025; Accepted 6 April 2025
Available online 11 April 2025

factors controlling soil OM mineralisation at the micro-scale is therefore a prerequisite for predicting C dynamics and for climate smart farming systems.

At the micro-scale, the complex arrangement of minerals, OM, and pores creates spatial heterogeneities that are more or less favourable for the soil microbial communities (Erktan et al. 2020). The pore network is the habitat of the soil microbial communities, and differences in pore sizes and pore connectivity determine water storage, substrate accessibility, aeration, and trophic interactions (Erktan et al. 2020; Rabot et al. 2018; Nunan et al. 2017). Under field conditions, macropores are often drained and biological activity is limited by the scarcity of water, while microbial activity in small micro- and nanopores is more likely limited due to size restrictions and by anoxic conditions (Keiluweit et al. 2016; Keiluweit et al. 2017). Oxygen availability, the spatial distribution of OM and differences in its microbial access to different parts of the pore network also influence microbial activities, such as the mineralisation of OM (Keiluweit et al. 2016; Keiluweit et al. 2017; Nunan et al. 2017; Shi et al. 2021). Enzyme activities have been found to be significantly higher in pores with radii between 30 and 150 μm than in other pore size classes (Kravchenko et al. 2019). In addition, root exudates and particulate organic matter (POM) are sources of labile OM and can create microbial activity hot spots (Kuzyakov and Blagodatskaya 2015). As a result of these pore scale interactions, soil organisms and their activities are sensitive to changes in land management practices (Doran and Zeiss 2000; Longepierre et al. 2021). Zuber and Villamil (2016), for example, showed in their *meta*-analysis that long-term no-till can cause a significant shift in the composition of microbial communities and that reduced tillage intensity promoted larger microbial biomass and greater enzymatic activity. However, they also showed that large variations in microbial properties could not be explained by environmental factors such as annual precipitation or soil texture and concluded that there is a need to fill knowledge gaps related to soil habitat constraints.

In arable fields, the pore network and microsites of the surface soil are affected by the applied tillage method (Bronick and Lal 2005; Munkholm et al. 2008; Schlüter et al. 2018), the crop cover (Lucas et al. 2019; Munkholm et al. 2013) and abiotic drivers such as freezing/thawing or wetting/drying (Diel et al. 2019; Klöffel et al. 2024; Leuther and Schlüter 2021). Conventional tillage disrupts the physical structure of soil in the top 25 to 30 cm each year and typically leads to an overall reduction in bulk density, a well-aerated soil and the incorporation of plant residues. The freshly created soil structure contains dense soil clods, larger macropores, and plant residues (Schlüter et al. 2018). In systems with reduced tillage, the top 5 to 10 cm are also disturbed each year during seedbed preparation, but crop residues often remain on the soil surface. Below 10 cm, the soil structure develops over the long-term, with biotic and other abiotic drivers affecting the development of soil structure (Leuther et al. 2023). The pore system without mechanical disturbance is often characterised by a well-connected network, where roots tend to explore existing macropores (Lucas et al. 2019).

In recent years, new methods have improved our understanding of the connection between soil structural properties and the spatial distribution of POM with respect to C storage and mineralisation rates (Arellano-Caicedo et al. 2021; Kravchenko et al. 2019; Rabbi et al. 2016), leading to improved modelling of soil OM turnover at different scales (Meurer et al. 2020b; Vogel et al. 2015; Zech et al. 2022). For instance, X-ray computed tomography (X-ray CT) analyses of soil structure at the micro-scale in combination with measurements of soil respiration and N_2O emissions have shown how interactions between microbial activity and soil structure can affect these activities (Ortega-Ramírez et al. 2023; Schlüter et al. 2022a). However, the different studies have revealed varying predictive power of structural indicators, which may be attributable to the focus on specific biological processes. In contrast to both respiration and N_2O emissions, calorimetric measurements include all biological activity in soils, which might give a more comprehensive view of the relationship between soil structure and microbial activity (Herrmann et al. 2014).

The aim of this study was to investigate the long-term effect of contrasting agricultural soil management practices on both soil structure and biological activity by combining X-ray CT soil structure analyses with isothermal calorimetry measurements. Undisturbed soil cores were taken from a field experiment which compared four agricultural management practices (conventional *vs.* reduced tillage each with either maize or winter wheat as the main crop), and structural indicators were determined using X-ray CT at a voxel resolution of 15 μm. Biological activity was measured by heat dissipation in response to water or glucose solutions added to different pore size classes. This was done to assess the importance of soil structural properties in determining biological activity in different parts of the pore network i.e. in pores with radii ranging from 15 to 75 μm and from 3 to 75 μm. The underlying hypothesis was that 12 years of contrasting agricultural management practices would affect soil structure and the accessibility of C sources to microbial communities. Therefore, we distinguished between native organic C solubilised and mobilised by water addition or externally added C by glucose solution.

2. Material and methods

2.1. Study site and sampling

Soil samples were taken from a field experiment situated in Säby, Sweden (R4-0009, 59°49'N, 17°42'E) (Bergkvist et al. 2011). It was established in 2010–2011 on a Cambisol formed on postglacial sediments with a silt loam texture (15 % clay, 55 % silt, and 30 % sand). The experiment consists of 12 treatments, replicated four times in a fully randomised block design (each plot size: 21 m wide and 20 m long; Fig. 1b). Soil samples were taken from all replicate plots of two different cropping rotation systems (i) with two different tillage regimes (ii):

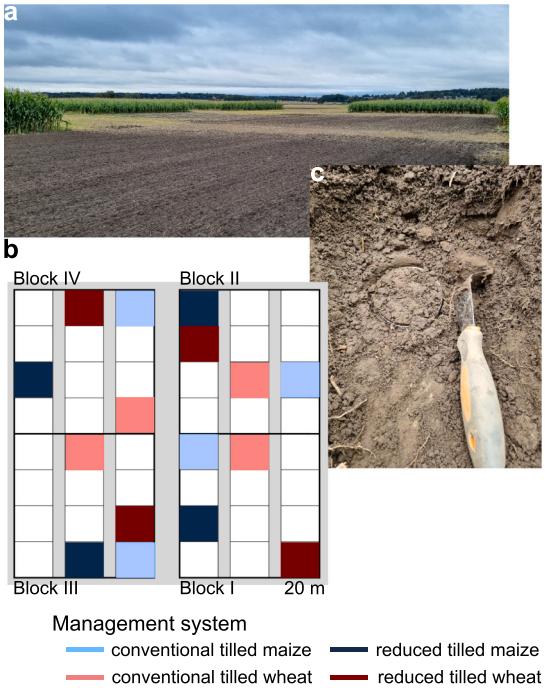

Fig. 1. Experimental field site at the time of sampling: maize is close to harvest and winter wheat has just been sown (a). Representation of the block design experiment R4-0009 at Säby (b), Sweden, showing the spatial distribution of conventionally tilled maize (light blue), conventionally tilled winter wheat (light red), reduced till maize (dark blue), and reduced till wheat (dark red). Sampling of a 17.2 cm^3 intact soil core (c).

(i) The two crop rotation systems were *winter wheat* as the main crop with flax, winter rapeseed and pea as break crops, and *maize* as the main crop with flax, summer rapeseed and pea as the break crops. At the sampling date in October 2022, the plots in the winter wheat crop rotation had been freshly tilled, harrowed and seeded with winter wheat after pea, whilst the maize crop rotation plots were just before harvest (Fig. 1a).

(ii) The two different tillage regimes were *conventional, inversion tillage,* which includes ploughing and disk harrowing and affects soil structure in the upper 28 cm and *reduced, non-inversion tillage*, where only the upper 10 cm are affected. Thus, the soil structure in the conventional tillage treatment was disturbed every year, while that in the reduced tillage plots was the result of twelve years of crop rotations. Samples were taken at a depth of 15–20 cm to analyse the topsoil below the annual disruption of the reduced tillage treatment.

Samples covered a range of potential soil structures from more crop-driven reduced tillage to more tillage-driven conventionally ploughed soil, shortly after and six months after seedbed preparation.

Undisturbed soil cores were collected randomly from each field plot at a depth from 15-20 cm using one 203.6 cm^3 steel cylinder (r = 3.6 cm, h = 5.0 cm) and three 17.2 cm^3 aluminium cylinders (r = 1.35 cm, h = 3.0 cm, Fig. 1c) within a 6 x 21 m zone, thus avoiding the outer 1.5 m of each plot. In addition, 1 kg bulk soil from the same depth was taken near the soil cores. After sampling, bulk soil and the small soil cores were stored in a freezer at −20 °C for maximum of four months before use. Samples were slowly thawed and stored in a fridge at 4 °C for two days prior to measurements, i.e. X-ray CT scanning, pre-incubation, and calorimetric measurements (Fig. 2).

2.2. Soil water retention and bulk properties

Soil water retention at suctions ranging from −10 to −500 hPa were determined for the 203.6 cm^3 samples using a suction plate. Samples were first saturated for two days and drained stepwise to −10, −30,

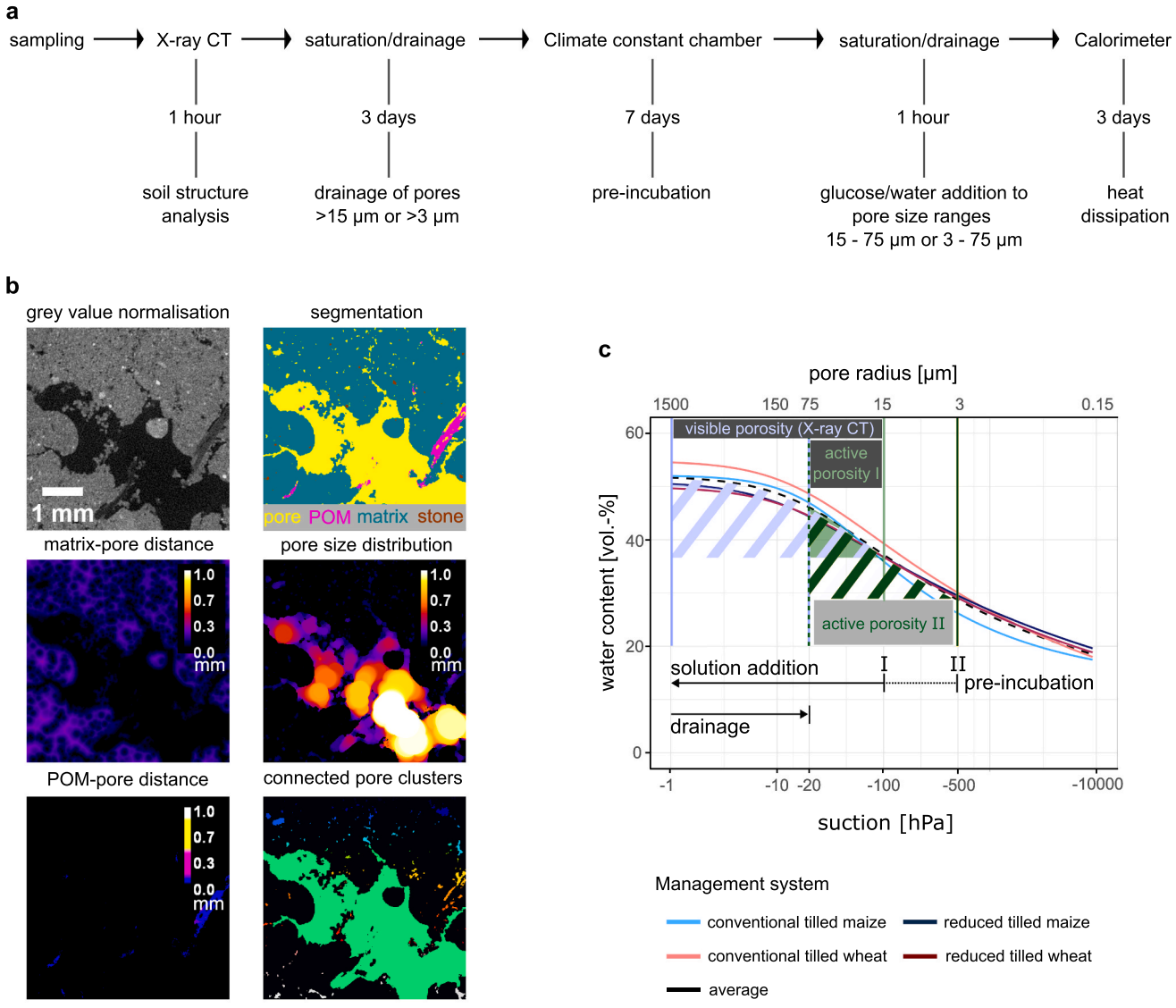

Fig. 2. Workflow for each 17.2 cm^3 soil core from sampling, image analysis, pre-incubation, solution addition to heat dissipation (a). Given time periods refer to the time span needed for each experimental step after thawing of the samples for two days in a fridge at 4 °C. The image shows the segmentation of a sub-volume containing the different soil constituents and the processing to measure various soil structure indicators (b). The mean soil water retention curves of the four agriculture management systems and the mean soil water retention curve for all plots (c, dashed line). The arrows indicate the range of water potentials covered by the glucose solution and water additions. The visible pore size range is defined by the resolution limit by X-ray CT (r = ≥15 µm), the active porosities are defined by the pore size ranges to which water and glucose solution were added (experiment I: 15 – 75 µm; experiment II: 3 – 75 µm).

−100, −300, and −500 hPa over a period of five weeks. Subsequently, samples were dried at 105 °C to calculate the bulk density. The van-Genuchten model (van Genuchten 1980) was fitted to the average soil water retention curves (Fig. 2c) using the *soilphysics* package in R (Da Silva and Lima 2015). This pre-measurement characterised the drainage behaviour of soil cores taken under different land management systems to evaluate the water content at different stages during the incubation experiment of the 17.2 cm^3 soil cores. Total organic carbon (TOC) and total nitrogen (TN) were determined on air-dried sieved bulk soil by dry combustion (TruMac CN, Leco corp, USA) according to ISO10694 and ISO13878, respectively.

2.3. Soil structure

Imaging was carried out with an industrial X-ray CT device (phoenix v|tomex|x m, GE, Germany). The 17.2 cm^3 soil cores were scanned for 53 min using a 0.1 mm copper filter at 100 kV and 150 μA, resulting in 2,000 projections (0.5 s per projection, 2 frames per projection). A voxel resolution of 15 μm was achieved at a 16-bit grayscale resolution in the reconstructed tomogram. Image processing and analysis were done with the software packages Ilastik pixel classification (Berg et al. 2019), FIJI ImageJ V1.53 (Schindelin et al. 2012), and R Studio (R Core Team 2020). An example of the image processing workflow is provided in Fig. 2b.

Soil samples were segmented via Ilastik pixel classification (https://www.ilastik.org), an interactive tool based on machine learning. Here, a random forest classifier was trained on the raw images by the user for different pixel class attributes, such as grey value and intensity gradients. Before image segmentation, the image size and the grey value distribution of the CT images were adjusted to the soil material to gain maximum contrast between background noise, i.e. air-filled area outside the sample cylinder was set to a grey value of 0, and highly dense material such as quartz particles, where about 0.02 vol-% of the brightest voxels were combined to the maximum intensity of a 16-bit image. For further processing, the images were converted to an 8-bit grayscale image. Subsequently, a training dataset for Ilastik pixel classification was prepared by selecting 10 sub volumes (400 × 400 × 400 voxel) from different samples where all structural features observed in the μCT images were present. Based on the training dataset, the samples were segmented into pores, organics, soil matrix, stones, and cylinder wall with an out-of-bag estimate of error rate of 2.44 %. The voxel grey value in an X-ray CT image results from the radiation attenuation by the object and is therefore dependent on the density and composition of the integrated material. Since mineral composition is assumed to be homogenously distributed in a randomised field experiment and the majority of the total pore space was below the detection limit of the X-ray CT (Fig. 2c), differences of the matrix grey value in a normalised image can be attributed to variations in the amount of material of low density, such as pores and organic matter, below the detection limit (Leuther et al. 2022). In order to analyse and compare the grey value of the soil matrix as an indicator for porosity and OM that were below the detection limit, the image grey values were normalised by linear rescaling between invariable material classes, i.e. air-filled pores and the aluminium cylinder wall. These were used as reference materials with fixed grey values of 20 and 160, respectively (Schlüter et al. 2022b). Areas in both reference materials (cylinder wall n > 5, pores n > 8) were selected by the ROI Manager in Fiji ImageJ to calculate the normalisation for each image. Finaly, the average normalised grey value of all voxels classified as soil matrix per sample were calculated.

The segmented pore class was analysed for standardised pore characteristics (Vogel et al. 2010; Weller et al. 2022). The visible macroporosity, the distance between voxels classified as pores, the pore size distribution, and two different pore connectivity characteristics were determined with Fiji ImageJ (Fig. 2b). The pore size distribution was computed by the maximum-inscribed sphere method (Doube et al. 2010). The visible pore size range was defined by the resolution limit by Xray CT (r = ≥15 μm) and the active pore size ranges were defined by the pores where water and glucose solution were added (r = 15 – 75 μm). Please note that the active porosity I (Fig. 2c) was within the range of the visible porosity, while pores with radii r = 3 – 15 μm as part of active porosity II (r = 3 – 75 μm) were below image resolution. The connectivity of the pore network was described by the connection probability (Γ) and the Euler number density (χ). The dimensionless Γ-indicator reflects the probability that two randomly chosen pore voxels belong to the same pore cluster (Renard and Allard 2013) and was calculated by equation (1):

$$\Gamma(p) = \frac{1}{n_p^2} \sum_{i=1}^{N(X_p)} n_i^2 \quad (1)$$

where n_p is the total number of pore voxels in the analysed volume X_p, n_i is the number of pore voxels per cluster, and $N(X_p)$ the maximum number of clusters. The χ value was calculated with the MorphoLibJ plugin (Legland et al. 2016). It quantifies pore connectivity as the number of isolated pores minus the number of redundant connections plus the number of cavities, expressed as a density [mm^{-3}]. The same plugin was used to determine the pore surface density [mm^{-1}]. The segmented pore image was used to calculate the frequency distribution of Euclidean distances from each voxel classified as solid material (i.e. organics, matrix, and stones) to the closest pore. The frequency of each pore size and distance between pores were used to calculate their average pore sizes and pore distances as weighted means.

POM can be present in the soil in different shapes and sizes (Leuther et al. 2022). In some cases, fractured organic particles are in a transition to be embedded in the soil matrix where image segmentation becomes challenging. In order to use the POM volume as a robust structural indicator, we excluded small, isolated POM clusters from the analysis. Therefore, we filtered the organics class with a Median 3D filter, to fill holes and to remove isolated voxels, and excluded POM clusters < 3.38 × 10^{-3} mm^3 (i.e. 1,000 voxels) by using connected component labelling of the MorphoLibJ plugin (Legland et al. 2016). POM was quantified as vol.-% for the entire sample. The distance of classified POM voxels to the nearest pore was calculated as an indicator for the state of POM-occlusion within soil matrix.

Soil structural properties were determined for the entire soil core and subsequently related to heat dissipation. Small disturbances at the edges due to sampling were excluded by region of interest definition after visual inspection to compare structural properties in response to the different management practices. The indicators were normalised by the analysed volume to account for volumetric differences.

2.4. Isothermal calorimetry

Studies measuring biological activities of the soil microbial communities, i.e. CO_2 respiration and heat dissipated, are routinely carried out on sieved, homogenised soil samples (Barros Pena 2018; Herrmann et al. 2014; Herrmann and Bölscher 2015), where soil conditions are optimised. In the present study, we adapted this method in order to explore biological activity in undisturbed soil columns with large pores filled with air (pore radius > 75 μm) and smaller pores filled with substrate solutions, i.e. glucose solution as C substrate or water in either pore radius between 15–75 μm or 3–75 μm, active pores I and active pores II, Fig. 2c). The aim of these adaptations was to distribute the substrate solutions into two targeted pore size classes within the sample in a very short time. This was achieved by capillary forces, saturation, and setting a certain suction at the lower boundary of the intact soil cores. We aimed to add in total 350 μg Glucose-C per gram soil, a substrate concentration that is sufficient to obtain a reliable calorimetry signal, as previous studies have shown (Harris et al. 2012). A glucose solution (0.037 M) was added to four replicate cores and tap water was added to two replicate cores for each soil management and pore size

class treatment. Tap water was used to prevent clay minerals from dispersing. Depending on the pore size class targeted, cores were pre-incubated at −100 hPa (r = 15 μm) or −500 hPa (r = 3 μm). In total, 24 cores were prepared for each pore size class. The laboratory experiment was done after the X-ray CT imaging and consisted of the following steps (Fig. 2a):

Pre-incubation: Undisturbed soil cores were saturated with tap water by capillary rise for 90 min, and fully saturated for 10 min. The samples were then drained for 3 days on a suction plate either at −100 hPa or −500 hPa to fill the pores smaller than the investigated range (radii < 15 μm and < 3 μm, respectively) with water (Fig. 2c). Subsequently, samples were pre-incubated at 20 °C for 1 week in a large plastic bag containing a wet tissue to prevent water loss through evaporation. The plastic bags were ventilated once a day to prevent the environment becoming anoxic.

Solution addition: After the pre-incubation period, samples were saturated with either tap water or a 0.037 M glucose solution by capillary rise for 30 min, followed by a full saturation for 10 min (Fig. 2c).

Drainage: The saturated soil cores were placed on a sand-bed for 20 min to drain larger macropores. Based on the soil water retention curve (Fig. 2c), it was estimated that samples reached a moisture content equivalent to −20 hPa, i.e. pores > 75 μm were air filled and the solution remained in pores with radii between 15 and 75 μm (active porosity I, Fig. 2c) and to pores with radii between 3 and 75 μm (active porosity II, Fig. 2c).

Incubation: The drained soil cores were placed in a 120 mL glass reaction vessel and immediately inserted into a TAM Air isothermal calorimeter (TA Instruments, Sollentuna, Sweden) set to 20 °C. The heat dissipation detection limit was 2 μW. Heat dissipation was continuously measured over a 70 h-period at 60 s intervals.

Drying: After each experimental step sample weights were recorded to determine the change in water content. At the end of the incubation experiment, samples were placed in an oven at 105 °C to obtain dry soil mass of each cylinder. The changes in water content for each step of the experiment conducted with the 17.2 cm^3 soil cores were estimated based on the soil water retention curve obtained with the 203 cm^3 soil cores (Fig. 2c).

Two different indicators were calculated from the calorimetric measurements: (i) the total biological activity as determined by the integral of heat dissipated between 4 and 62 h, and (ii) the dynamics of the system which was estimated as the time elapsed when 50 % of total heat had dissipated (Dufour et al. 2022). The latter indicator gives information on the rate with which the microbial communities respond to the availability of substrate. The starting time was set to 4 h to allow the soil to equilibrate and the end time was set to 62 h avoiding any oxygen depletion in the glass reaction vessels (Barros Pena 2018).

2.5. Statistical analysis

Data management, data analysis and figures were all carried out using the open-source packages *tidyverse* (Wickham et al. 2019) and *ggplot2* (Wickham 2016) in R Version 4.1.2 (R Core Team 2020). The comparisons of means for each soil property were done using an ANOVA in the *rstatix* package (Kassambara 2020). Bulk soil properties were measured for every plot. The results per plot were used to test for differences between the treatments (n = 4). Undisturbed samples taken from within each plot were treated as technical replicates (n = 3) and their average values per plot as true replicates for ANOVA comparison (n = 4). Variables were tested for normality and homogeneity of variance by the Shapiro-Wilk test and Levene's test, respectively. Where the requirements for an ANOVA were not fulfilled, the significance of differences was tested by a Kruskal-Wallis test with Bonferroni p-adjustment, as implemented in the *agricolae* package (Mendiburu and Yaseen 2020). Correlation matrices were created to correlate X-ray CT indicators and isothermal calorimetry measurements with each sample treated as an independent individual. Regressions among variables were determined using the *ggpubr* package (Kassambara 2020). The multivariate regression method Partial Least Squares Regression (PLSR), implemented in the *pls* package (Mevik and Wehrens 2007), was used as an exploratory analysis tool to select suitable predictor variables for total heat dissipation and the rate of activity, the latter indicated by the time required to dissipate 50 % of the total heat. PLSR accounts for co-correlations between variables.

3. Results

3.1. Impact of soil management on bulk properties and soil structure

Conventional tillage significantly increased visible volumetric POM content and decreased matrix grey values in both cropping rotation systems (Table 1). The matrix grey values, which likely vary with porosity and OM below the resolution of the scans, correlated negatively with the POM volume ($r^2 = 0.42$, $p < 0.01$). The bulk soil TOC and TN (measured on air-dried, milled < 2 mm soil samples) did not differ significantly between the cropping systems. The average distance between POM and the nearest visible pore was greater in the conventional tillage treatment than in the reduced tillage treatment. This was most evident in undisturbed soil cores taken from the freshly ploughed winter wheat plots where large volumes of POM were visible. While the segmented POM volume in reduced tilled plots often consisted of roots and smaller residues, the conventionally tilled plots contained litter and seed structures embedded in the soil matrix. These POM structures were also visible in the maize plots at the end of the growing season, about five months after seedbed preparation (Fig. 3b). In general, the POM-pore distance increased with POM volume ($r^2 = 0.53$, $p < 0.01$).

The soil from the maize rotation system showed a more connected pore network, with high visible porosity (14 vol-%) and Γ-connectivity (0.8), compared to the soil under winter wheat (7 vol-% and 0.5, respectively). The differences in pore size fraction with radii between r = 15 and 75 μm were smaller in the soil under winter wheat (4 vol-%) than under maize (6 vol-%). Within a cropping rotation system, conventional tillage produced a mixture of denser soil clods and loosely packed soil (see examples in Fig. 3a). This resulted in shorter distances between pores, smaller pore sizes and higher number of isolated pores (Table 1). Visual inspection showed that reduced tillage resulted in a more homogenous distribution of earthworm casts and densely packed aggregates (Fig. 3a) with low amounts of visible porosity between a well-connected pore system containing larger macropores (Table 1). The pore surface density was significantly higher in the maize rotation system, but also systematically lower in the reduced soil tillage regime compared to the conventionally tilled soil. The pore surface was therefore affected by both tillage and cropping rotation system. It was also positively correlated with the visible porosity ($r^2 = 0.69$, $p < 0.001$). The visible (r ≥ 15 μm) and active porosity (r = 15 – 75 μm) measured by X-ray CT were comparable to the volumetric contents determined from the soil water retention curve (Fig. 2c). The overall bulk density showed a similar tendency of more loosened soil under conventional ploughing than reduced tillage but did not significantly differ between the treatments because of high variances within the treatments. Soil texture and textural porosity should be considered the same for all treatments in the experiment due to the randomized plot design. Therefore, it can be assumed that most differences in pore networks occurred within the structural porosity, which was quantified with the visible porosity range and the porosity below the resolution partially integrated in the matrix grey value.

3.2. Heat dissipation in soil cores from different soil management systems

The heat dissipation after glucose addition to pore sizes ranging from 3 to 75 μm was significantly higher under maize than winter wheat, regardless of the tillage regime ($p < 0.01$; Table 2). It should be noted that the amount of glucose solution retained in the samples was also

Table 1
Characterization of physicochemical indicators in soil taken from a depth of 15 − 20 cm in response to different agricultural management practices. Indicators were categorised into organic matter (OM) and pore characteristics. Values in parentheses are standard errors, letters and p-value represent statistical significance of ANOVA or Kruskal-Wallis tests.

Reference	Crop rotation Tillage regime	Maize conventional	reduced	Wheat conventional	reduced	p-value
		n = 4	n = 4	n = 4	n = 4	
Bulk soil	Bulk density [g cm^{-3}]	1.27 (0.02) ^{a}	1.33 (0.03) ^{a}	1.28 (0.03) ^{a}	1.37 (0.05) ^{a}	0.159
X-ray CT	Matrix grey value [-]	107.4 (1.47) ^{bc}	112.5 (1.08) ^{ab}	106.4 (0.59) ^{c}	114.5 (1.94) ^{a}	<0.01
	OM characteristics					
Bulk soil	Total org. Carbon [g 100 g^{-1}]	2.46 (0.07) ^{a}	2.54 (0.09) ^{a}	2.60 (0.11) ^{a}	2.49 (0.05) ^{a}	0.662
Bulk soil	Total Nitrogen [g 100 g^{-1}]	0.22 (0.01) ^{a}	0.23 (0.01) ^{a}	0.21 (0.01) ^{a}	0.21 (0.01) ^{a}	0.609
X-ray CT	Particulate OM [vol.-%]	0.39 (0.07) ^{ab}	0.15 (0.02) ^{b}	0.66 (0.13) ^{a}	0.22 (0.09) ^{b}	<0.01
X-ray CT	POM-pore distance [mm]	0.04 (0.00) ^{ab}	0.03 (0.01) ^{b}	0.05 (0.01) ^{a}	0.04 (0.00) ^{ab}	<0.05
	Pore characteristics					
X-ray CT	Visible porosity [vol.-%]	14.29 (1.2) ^{a}	13.03 (0.3) ^{a}	7.50 (0.7) ^{b}	7.08 (0.9) ^{b}	<0.001
X-ray CT	Active porosity [vol.-%]	6.75 (0.92) ^{a}	6.12 (0.31) ^{ab}	4.35 (0.43) ^{b}	3.72 (0.36) ^{b}	<0.01
X-ray CT	Mean pore size [mm]	0.22 (0.04) ^{ab}	0.32 (0.08) ^{a}	0.12 (0.01) ^{b}	0.32 (0.17) ^{ab}	<0.05
X-ray CT	Mean pore distance [mm]	0.08 (0.01) ^{b}	0.10 (0.01) ^{ab}	0.10 (0.00) ^{ab}	0.13 (0.02) ^{a}	<0.05
X-ray CT	Surface density [mm^{-1}]	4.91 (0.59) ^{a}	3.67 (0.22) ^{ab}	2.92 (0.19) ^{b}	2.41 (0.31) ^{b}	<0.01
X-ray CT	Euler number χ [mm^{-3}]	104.5 (19.5) ^{a}	52.7 (8.8) ^{a}	79.5 (7.1) ^{a}	63.2 (12.7) ^{a}	0.070
X-ray CT	Γ-connectivity [-]	0.77 (0.05) ^{a}	0.83 (0.03) ^{a}	0.45 (0.15) ^{b}	0.63 (0.04) ^{ab}	<0.001

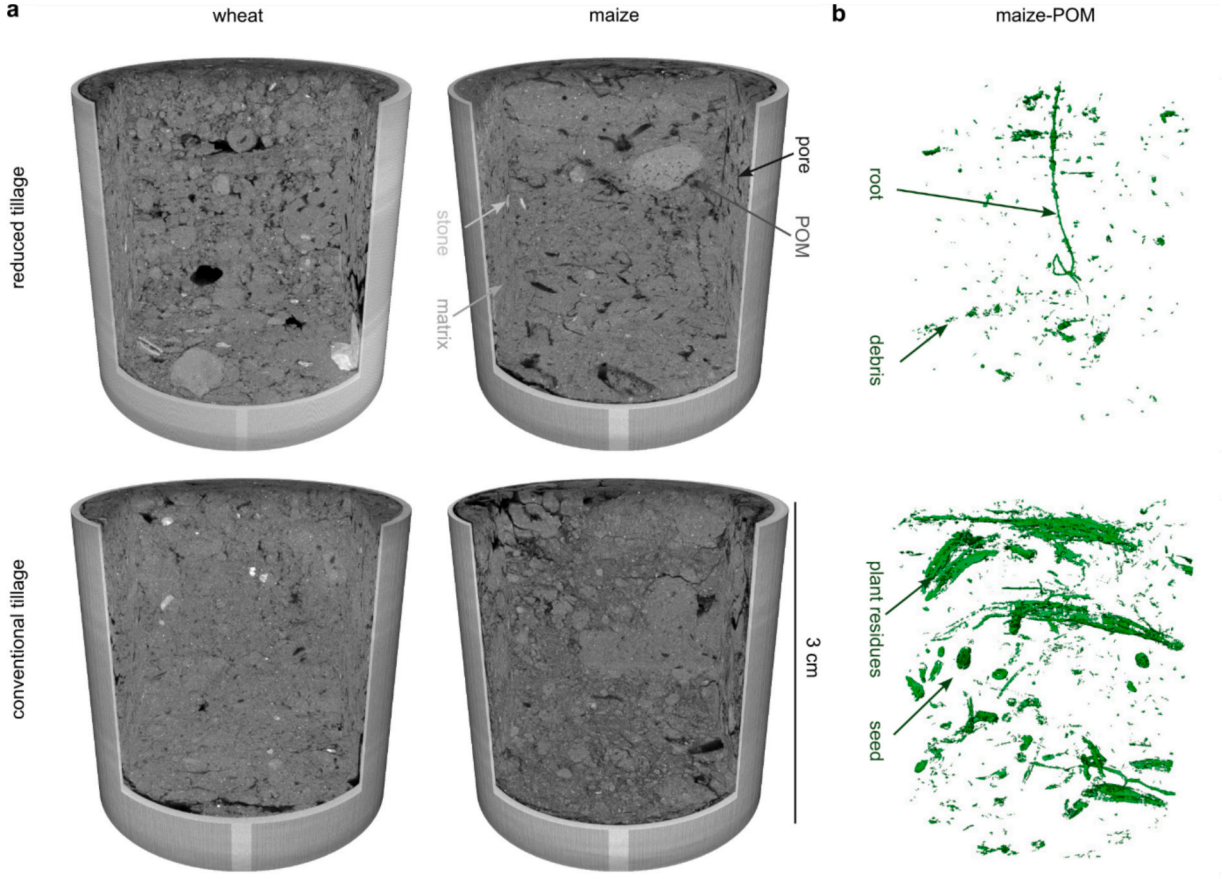

Fig. 3. Representative X-ray CT tomograms of the investigated management systems (a). Segmented POM fractions of the reduced and conventional tilled maize tomograms (b), respectively.

significantly higher in undisturbed soil cores taken from the conventionally tilled maize plots ($p < 0.05$, Table 2). The dynamics of the systems, i.e. the time elapsed for 50 % total heat to be dissipated, did not differ significantly between treatments ($p = 0.108$). When glucose was added to pores in the 15–75 μm class, the differences between the four management systems were not significant. Heat dissipation profiles are presented as time series in the supplementary material (Fig. S1: 15–75 μm pore size range, Fig. S2: 3–75 μm pore size range).

The patterns were slightly different when water was added to the samples instead of glucose solution. As with the glucose additions, significantly higher amounts of water were retained in the conventionally tilled maize samples than in the winter wheat samples ($p < 0.05$, Table 3) when water was added to the 3–75 μm class. This did not result in a higher total heat release but did result in a significantly longer time until 50 % of total heat was dissipated ($p < 0.01$). Again, no significant differences were found for any of the indicators when water was added

Table 2
Mean values of heat dissipation (J g^{-1} soil) during 58 h incubation at 20 °C after glucose addition. Values in parentheses are standard errors, n = number of field plots tested, p-values represent statistical significance of ANOVA and Kruskal-Wallis tests.

Crop rotation	**Maize**		**Wheat**		
Tillage regime	**conventional**	**reduced**	**conventional**	**reduced**	**p-value**
Pore range: 15 – 75 µm	n = 4	n = 4	n = 4	n = 4	
Glucose solution [ml]	0.61 (0.13) [a]	0.44 (0.07) [a]	0.33 (0.08) [a]	0.65 (0.21) [a]	0.350
Total Heat [J g^{-1} soil]	2.85 (0.98) [a]	2.95 (0.31) [a]	2.47 (0.39) [a]	2.55 (0.92) [a]	0.955
Time 50 % [h]	20.47 (1.62) [a]	17.44 (1.73) [a]	20.98 (1.14) [a]	21.25 (1.39) [a]	0.301
Pore range: 3 – 75 µm	n = 4	n = 4	n = 4	n = 4	
Glucose solution [ml]	1.53 (0.19) [a]	1.11 (0.08) [ab]	0.69 (0.18) [b]	0.76 (0.18) [b]	<0.01
Total Heat [J g^{-1} soil]	6.08 (1.24) [a]	4.44 (1.73) [a]	2.48 (0.33) [b]	2.48 (0.92) [b]	<0.01
Time 50 % [h]	24.95 (1.77) [a]	25.83 (1.96) [a]	19.42 (2.02) [a]	19.41 (2.13) [a]	0.108

Table 3
Mean values of heat dissipation (J g^{-1} soil) during 58 h incubation at 20 °C water addition. Values in parentheses are standard errors, n is the number of field plots tested, p-values represent statistical significance of ANOVA and Kruskal-Wallis tests.

Crop rotation	**Maize**		**Wheat**		
Tillage regime	**conventional**	**reduced**	**conventional**	**reduced**	**p-value**
Pore range: 15 – 75 µm	n = 2	n = 2	n = 2	n = 2	
Water addition [ml]	0.62 (0.01) [a]	0.36 (0.06) [a]	0.58 (0.16) [a]	0.66 (0.01) [a]	0.253
Total Heat [J g^{-1} soil]	5.78 (4.02) [a]	2.43 (0.80) [a]	1.85 (0.82) [a]	0.71 (0.11) [a]	0.450
Time 50 % [h]	27.08 (12.3) [a]	18.19 (1.57) [a]	24.99 (6.04) [a]	29.07 (2.89) [a]	0.730
Pore range: 3 – 75 µm	n = 2	n = 2	n = 2	n = 2	
Water addition [ml]	1.66 (0.25) [a]	0.95 (0.13) [ab]	1.18 (0.17) [ab]	0.43 (0.05) [b]	<0.05
Total Heat [J g^{-1} soil]	5.15 (4.21) [a]	2.55 (0.08) [a]	2.09 (0.64) [a]	2.45 (1.09) [a]	1.000
Time 50 % [h]	34.00 (1.50) [a]	26.04 (1.37) [ab]	18.60 (2.68) [b]	21.09 (1.10) [ab]	<0.05

to the 15–75 µm pore size class. This may have been due to the high variability in the heat dissipation among maize crop replicates (Fig. 4a).

No significant differences between pore size ranges were found for either of the biological activity indicators, regardless of the management practice (Fig. 4). This was true for both glucose solution and water addition.

3.3. Heat dissipation and structural indicators

Correlation matrices for the experiments with undisturbed soil cores showed that multiple structural indicators correlated significantly with both activity metrics, i.e. total heat dissipation and the rate of activity (Fig. 5a, 5b). However, the calorimetric measurements were not correlated to any image-based OM indicators (i.e., POM volume, POM-pore distance). When glucose was added, heat dissipation increased significantly with visible porosity, active porosity, and pore density. When normalised by the amount of glucose solution added, all correlations disappeared, suggesting that heat dissipation depended on the amount of glucose solution retained in the active pores (r = 15 and 75 µm). The significant correlations between heat release and the grey value of the soil matrix in the soil cores that received glucose in the 3–75 pore size range indicate that pores smaller than 15 µm were also involved in heat production (Fig. 5b). For all samples including both pore size ranges, there was a positive correlation between glucose solution addition and heat dissipation ($r^2 = 0.5$, $p < 0.01$), which was not the case for water addition ($r^2 = 0.1$, $p = 0.26$). In soil cores that received water, the calorimetric metrics were significantly ($p < 0.001$) correlated to the active porosity and the pore surface density (Fig. 5c). Here, the distance between pores was an additional significant indicator, showing that denser areas reduced the overall heat dissipation. In

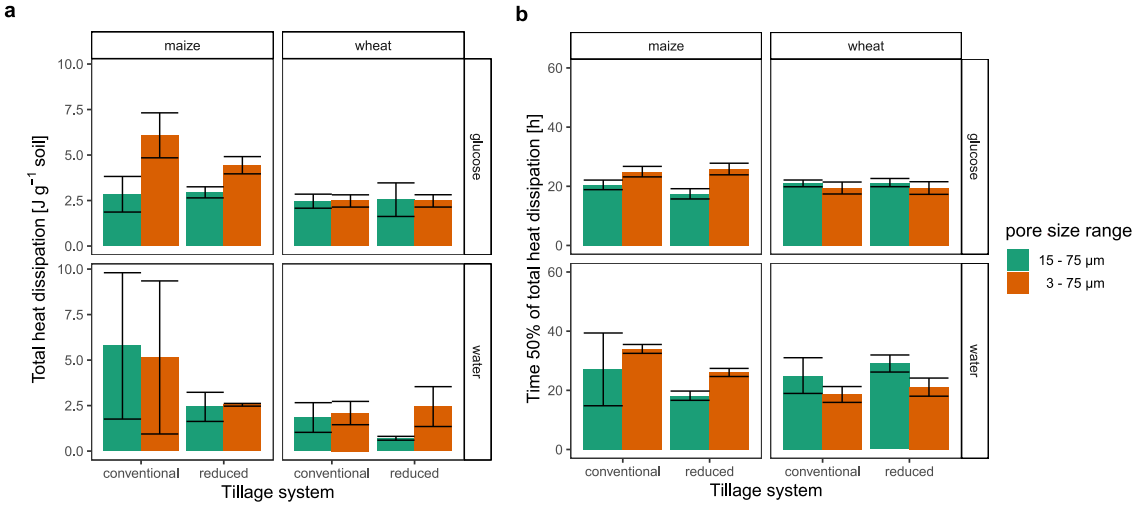

Fig. 4. Mean values of heat dissipation (J g-1 soil) during the 58 h incubations at 20 °C (a) and the time required to dissipate 50 % of the total heat (b). The error bars mark the standard error. No significant differences between the experiments with solution addition to the two pore size ranges within a management system were found.

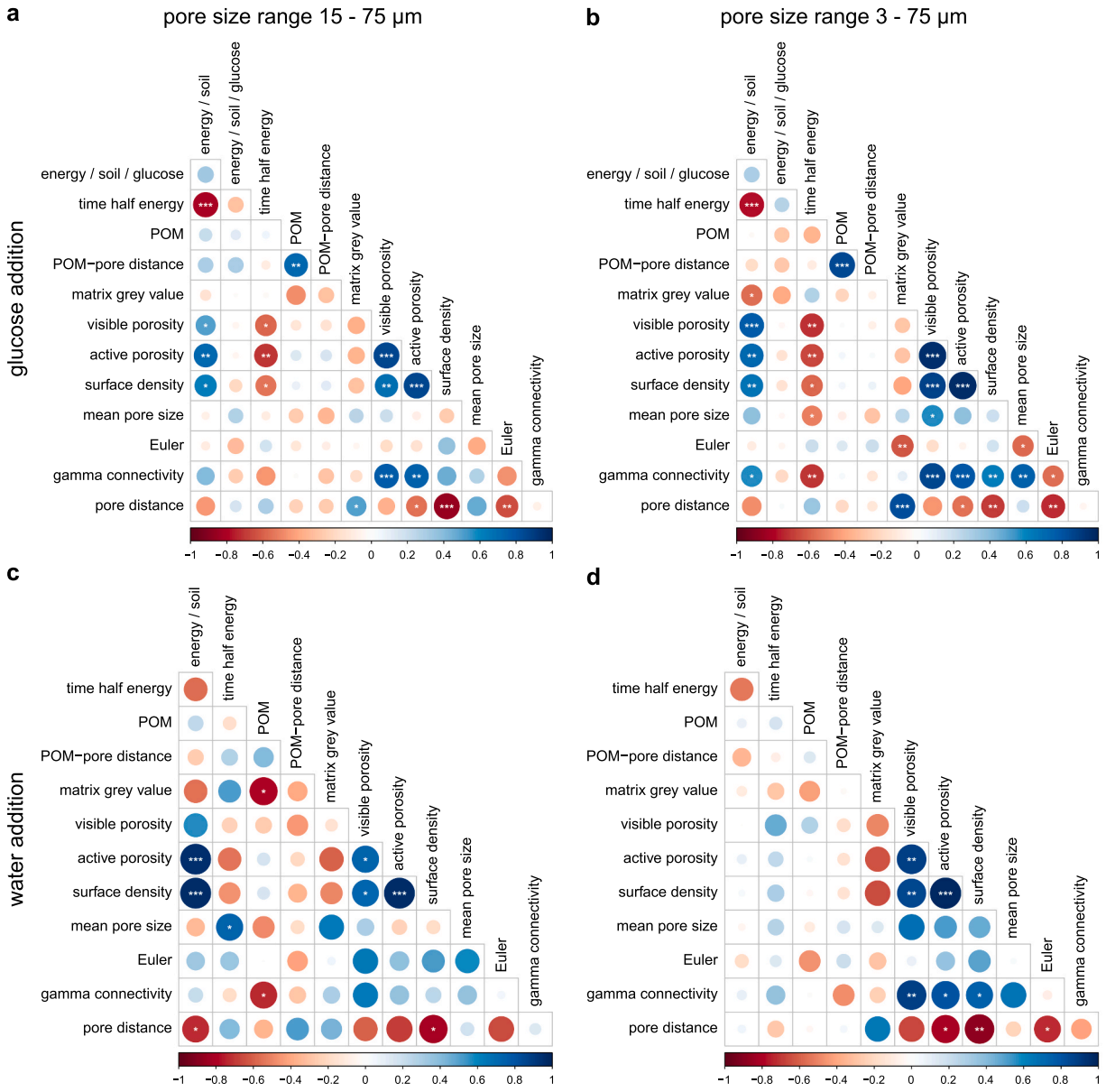

Fig. 5. Correlation matrixes of the different experiments with undisturbed soil cores after glucose (top, n = 16 per experiment) and water addition (bottom, n = 8 per experiment) to pores ranging in radii of 15 to 75 µm (left) and 3 to 75 µm (right). "Energy / soil" displays heat dissipated (J g^{-1} soil) during 58 h incubation at 20 °C, the time needed to dissipate 50 % of the total heat, i.e. the rate of activity, is displayed by "time half energy".

contrast, none of the structural indicators could explain heat dissipation in samples that received only water in the 3–75 µm pore size range (Fig. 5d).

We used PLSR analysis to combine pore network and OM indicators as predictor variables to explain the observed variances in heat dissipation (Table 4). In the glucose-amended samples, the predictive power of pore network indicators was 52 % and 58 % for total heat dissipation in the 15 – 75 µm and the 3 – 75 pore size range, respectively. The OM indicators could only explain < 10 % of the heat dissipation variance. If the grey value of the soil matrix is taken into account as an additional predictive variable for heat dissipation, the predictive power for the glucose-amended samples increased significantly to values ranging from 63 to 81 %. The prediction of differences in heat dissipation dynamics was less powerful for both experiments. In samples that received water to the 15 – 75 µm pore size range, the pore network indicators explained up to 94 % of the variance in total heat dissipation and 50 % of the dissipation dynamics but the indicators failed to explain the variances in samples that received water to the 3 – 75 µm pore size range. In both experiments with addition of water, the matrix grey value did not significantly improve the model performance.

4. Discussion

Various structural indicators showed that the studied agricultural management represents a large gradient in pore network and POM characteristics, including potential hot spots (roots and POM) as well as areas of potential physical constraints (waterlogged and air-filled pore spaces). While visible porosity and pore connectivity were mainly related to the cropping rotation system (maize > wheat), the tillage regime affected (i) the mean pore size (reduced > conventional), (ii) soil matrix grey value (reduced > conventional), and (iii) POM volume (conventional > reduced). Pore surface density and mean distances between pores were affected by both tillage regime and cropping rotation. It should be noted that the maize had not yet been harvested at the time of soil sampling, while winter wheat had just been sown and the field was lying 'fallow' (see Fig. 1a), i.e. conditions in the field differed

Table 4
Results of a Partial Least Square Regression analysis. Percentage of the variance in total heat dissipation and the time to dissipate 50 % of the energy explained by different structural and organic matter (OM) indicators.

	Pore network indicators (active porosity, surface density, pore distance)		OM indicators (POM, POM-pore distance)		Pore network indicators + matrix grey value	
	Energy/soil	Time 50 %	Energy/soil	Time 50 %	Energy/soil	Time 50 %
Glucose addition						
Pore range: 15 – 75 µm	52.1 %	6.5 %	8.6 %	25.3 %	62.8 %	10.2 %
Pore range: 3 – 75 µm	58.3 %	45.6 %	9.4 %	26.6 %	80.9 %	50.1 %
Water addition						
Pore range: 15 – 75 µm	94.0 %	50.0 %	20.0 %	7.7 %	94.6 %	62.8 %
Pore range: 3 – 75 µm	11.5 %	15.1 %	13.7 %	26.6 %	12.6 %	15.4 %

significantly between the two management systems. Consequently, differences in soil structure might be altered not only by the management system itself, but also due to differences in cropping stages. The soil cores provided a range of micro-habitats to test how different soil structural indicators affect the accessibility of C sources to microbial communities. Based on the results after glucose and water addition it can be summarised that:

(i) active porosity and pore surface density were the best pore network indicators of heat dissipation in experiments with both water and glucose additions to the pore size range 15 – 75 µm.
(ii) the grey value of the soil matrix, an indicator for pores and OM below the image resolution, increased the predictive power of heat dissipation up to 81 % after glucose addition for experiments conducted at the pore size range of 3 – 75 µm.
(iii) indicators for POM volume and POM occlusion did not provide significant information as an explanatory variable for the variance in heat dissipation for either pore size range or solute additions.
(iv) the time required to dissipate 50 % of the total heat was not correlated to most structural and POM indicators > 15 µm determined via X-ray CT; the combined predictive power of pore network indicators and matrix grey value was comparably low (10 – 63 %).

The effects of the tested pre-incubation condition (water filled pores ≤ 15 µm or ≤ 3 µm), visible pore structure and organic matter on biological activity after glucose and water addition is illustrated in Fig. 6 and discussed in the following.

4.1. The effect of pore structure on biological activity

The visible porosity > 15 µm partially quantifies the microbial habitat which is most favourable for soil microorganisms (Erktan et al. 2020). The pore surface describes the solid-pore interface where the microbial cells are expected to be mainly located (Young et al. 2008). A well-connected pore network can promote aeration, water and nutrient transport within the soil sample (Bhattacharyya et al. 2021; Longepierre et al. 2021). Within a cropping rotation system, conventional tillage resulted in shorter distances between pores, smaller pore sizes and a higher number of isolated pores, none of which significantly affected heat dissipation after glucose addition. As a result, no differences were found between the management practices. It is possible that the moderate bulk density of all treatments (p_b = 1.27 – 1.37) did not produce any limitation for glucose mineralisation in the analysed pore size ranges (Fig. 6a). However, experiments with glucose addition to the pore radius range between 3 and 75 µm provided additional information on how soil structure affects heat dissipation. The lower grey value of the soil matrix, which indicates the presence of more low density components (air or water filled pores as well as OM) below the resolution of the scans, was related to heat dissipation in the pore radius range between 3 and 75 µm, i.e. providing an indicator of biological activity in non-visible pores between 3 and 15 µm (Fig. 6b). A significant contribution to glucose mineralisation of this specific pore size range has also

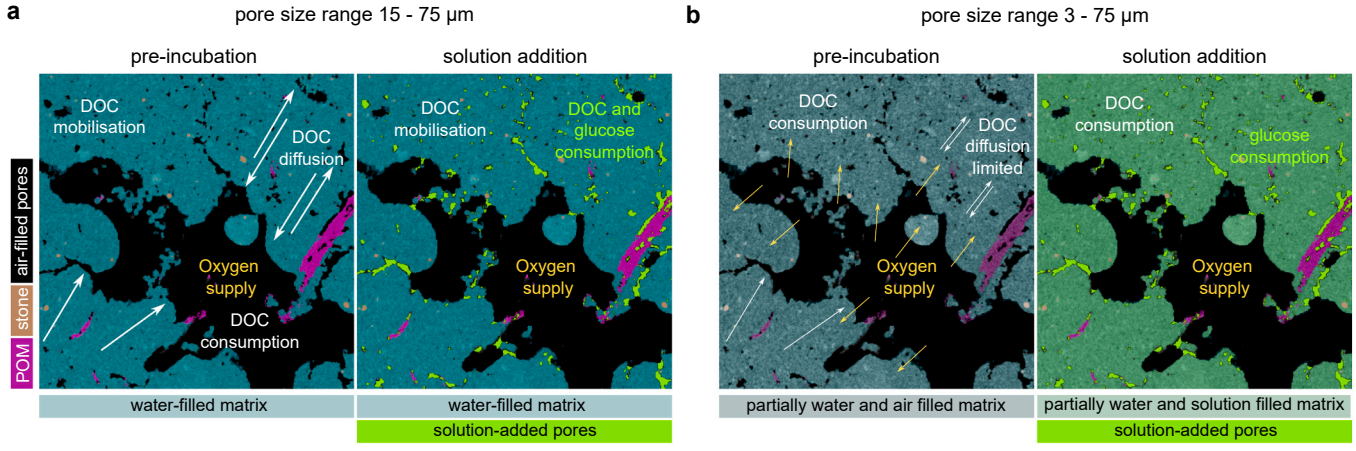

Fig. 6. Conceptual, graphical summary of the assumed condition in the tested pore ranges (a 15 – 75 µm, b 3 – 75 µm) during 7 days of pre-incubation and after substrate addition when heat dissipation was measured for 3 days. The illustration (6 x 6 mm) is based on an X-ray CT sub-volume gained at a voxel resolution of 15 µm. When the soil matrix (pores ≤ 15 µm) is water saturated (a) labile organic carbon can diffuse towards air filled pores space (indicated by the arrows) where biological activity is stimulated by oxygen supply. When glucose or water is added to the active visible pore space by saturation and drainage (15 – 75 µm), dissolved organic carbon (DOC) is also mobilized and transported towards the active pores where biological activity was stimulated during pre-incubation. When the soil matrix is partially water and air filled (b), oxygen can diffuse towards non-visible pores ≤ 15 µm indicated by the soil matrix grey value. DOC diffusion is limited by high tortuosity and air and DOC consumption is also stimulated in non-visible pores. Glucose consumption after substrate addition takes place mainly in the analysed pore space while the reduced mobility of DOC decouples the visible pore network from heat dissipation after water addition.

been observed by previous studies where similar pore size classes were associated with biological activity (Kravchenko et al. 2019). Furthermore, the pore connectivity was a significant predictor of the variability of heat dissipation in these experiments indicating the importance of gas and nutrient transport within the sample (Bhattacharyya et al. 2021). For larger soil cores, oxygen supply from the surrounding headspace to the inside of the core can be limiting and, in this case, pore connectivity may have affected oxygen diffusion rates (Keiluweit et al. 2016). Interestingly, the oxygen supply from the visible pore system towards the solution filled pores space in dense areas indicated by the matrix-pore distance did not significantly affect heat dissipation.

The experiment investigating the pore radius range between 3 and 75 μm showed that the combination of a favourable structure for soil organisms induced by both tillage regime and main crop, and the ability to retain more glucose solution resulted in significantly higher total heat dissipation for soil cores under conventional tilled maize plots compared to reduced tilled wheat plots. In this study, we covered a broad range of soil structures by sampling various management systems (main crop, tillage system) at different points of cropping stages (i.e. before harvest and after seedbed preparation). It is known that certain pore size classes are linked to biological activity in soils (Kravchenko et al. 2021; Kravchenko et al. 2019; Nunan et al. 2017). However, the results presented in this study indicate that small-scale habitats of soil organisms are complex systems which cannot be solely described by a simplified model of various pore size distribution as often observed in literature (Bodner et al. 2023). The study shows that in addition to the porosity in the visible pore size range, the pore geometry (pore surface density) and connectivity are equally important habitat characteristics and emphasise the significance of low-density areas for biological activity which can be evaluated based on the soil matrix grey value.

This becomes relevant especially in farming systems with soluble C-source applications, such as e.g. manure fertilisation, where the ability of a pore system to retain water against gravity in the pore size range between 3 and 75 μm might result in increased biological activity when oxygen supply is sufficient. Interestingly, we expected the maximum effect of tillage practices and plant residue incorporation in the winter wheat plots, since sampling was done shortly after field management while maize was still not harvested. However, no significant differences were found between the freshly ploughed and reduced tilled management practices. Fertilisation and root decomposition of the former crop (i.e. peas, in the case of winter wheat) might have provided sufficient nutrient input, as the large response of biological activity after water addition suggests, masking any potential differences.

4.2. *The effect of organic matter on biological activity*

In contrast to the TOC content, the annual incorporation of crop residues by conventional tillage resulted in a significant increase in OM indicators estimated by X-ray CT. It should be noted that in the TOC analysis, POM with a size more than 2 mm was excluded during sample preparation, which could explain this difference. Studies using density fractionation of OM on agricultural fields with a silty loam soil texture showed that 80 to 95 % of OC can be assigned to mineral-associated organic matter (John et al. 2005; Surey et al. 2020). Furthermore, it has been shown that POM quantified by X-ray CT is a significant source of water extractable OC (Leuther et al. 2022). The different results indicate that twelve years of contrasting soil management practices have not changed the amount of mineral-associated organic matter content, but have changed that of the more labile POM. The negative correlation between the matrix grey values and the POM volume indicates a positive impact of POM incorporation on background porosity and/or on OM below the detection limit in the matrix of the conventional tilled management system.

In plots with reduced tillage, roots serve as the primary source of POM. The shorter POM-pore distances indicate that they were located inside or close to pores, thus less occluded within the soil matrix and more readily available for microorganisms. The greater microbial access to crop residues due to tillage practice can lead to a stimulation of microbial activity (Zuber and Villamil 2016). However, neither the POM volume nor the POM-pore distance, i.e. indicators for potential hot spots and C sources, correlated with heat dissipation in any of the experiments independent of glucose solution or water addition. This contrasts with most recent studies, where POM mass (Schlüter et al. 2022a) and POM distance (Ortega-Ramírez et al. 2023) provided the best explanatory variable for basal CO_2 respiration in the field and N_2O emissions from intact soil cores, respectively. These studies were conducted at a coarser resolution (>30 μm) and used a similar conservative approach to segment POM in X-ray CT images. It can be assumed that we had a higher accuracy in segmenting POM due to the higher resolution and the training of a machine learning segmentation rather than simple grey value segmentation. This emphasises that in our study a source other than the detected POM volumes caused the high heat dissipation. For experiments with glucose additions, it can be argued that the high-energy content and readily available glucose for decomposition masked the influence of turnover of native soil OM. As discussed above, heat dissipation correlated with the amount of solution retained in the sample. However, in the water amended samples there were heat dissipation peaks comparable to those obtained with glucose addition and it is surprising that POM metrics were not related to these peaks. It is possible that significant amounts of OM were dissolved when preparing the samples and that biological activity was stimulated by this additional DOC mobilisation upon water addition (Fig. 6a).

It should be taken into account that maize plants were still in the field at the time of sampling, and roots and root exudates were most likely still a source of labile OM (Hermle et al., 2008; Furtak et al., 2017). This potential mobilised C source might explain the higher metabolic response in undisturbed soil cores taken from the maize plots. For the winter wheat plots, harvest of peas, soil aeration, and field preparation for winter wheat might have resulted in the decomposition of easily available OM in the field prior to soil sampling, resulting in lower heat dissipation during the laboratory experiments. For the experiments investigating the pore radius ranging between 15 and 75 μm, the pore space of visible soil matrix (pores < 15 μm) was saturated while the visible pore space was air-filled (Fig. 6a). The saturation of the pores below the scan resolution may have resulted in the mobilisation of labile OM imbedded in denser areas (soil matrix) and the diffusion towards the visible, air-filled pore surfaces. As the diffusion distance was likely related to the matrix-pore distance, the negative correlation between heat dissipation and matrix-pore distance suggests that the longer the diffusion distance, the lower the heat dissipation. Pre-incubation of samples at −500 hPa (pore radius range between 3 and 75 μm), however, reduced the amount of water-filled pore space in the soil matrix from 38 vol% to 30 vol% (calculation based on the soil water retention curve in Fig. 2c). This might have reduced overall mobilisation of OM and increased the diffusion path length towards the visible pore surfaces or resulted in a disconnected path (Fig. 6b). Furthermore, it likely enabled oxygen supply from larger, connected pores to the non-visible pore space and thus might have stimulated OM consumption in the partially water and air-filled pore space of the moil matrix during pre-incubation. The significant decrease in water filled pore space of the soil matrix during pre-incubation, and herewith the disconnection of diffusion path ways, might explain why the matrix-pore distance failed to predict heat dissipation in the water addition treatments at the pore radius range between 3 and 75 μm. Interestingly, in these experiments, the time needed to dissipate 50 % of the total heat was significantly shorter in the freshly ploughed winter wheat plots than in the maize plots. Again, all pore and POM indicators failed to predict the variance in total energy production. The results indicate that labile OM of different sources, rather than visible POM must have caused this pronounced energy production in the maize intact soil cores. In future studies, single aggregates could be used to investigate the influence of POM on heat dissipation at higher resolution (usually performed at a voxel resolution

between 4 – 8 μm). Sub-resolution OM within the soil matrix could be labelled with osmium as an additional measure to quantify spatial gradients in OM (Schlüter et al. 2022b) and water extractable OC quantification in the bulk soil could further increase our understanding of different OM sources as drivers for biological activity in intact soil structures. A longer pre-incubation time could also diminish the effect of labile OM on heat dissipation.

4.3. The measurement of biological activity in undisturbed soil cores using isothermal calorimetry

All biological systems produce heat proportionally to the rate at which chemical reactions or physical processes take place therein. In the past decade, the microbial energetics approach is an emerging method in exploring microbial activity and metabolism (e.g. Barros Pena 2018; Harris et al. 2012; Yang et al. 2024). Isothermal calorimetry is used to quantify heat dissipation from soil samples and thus to quantify energetics of the microbial communities in the soil samples. Hitherto, mainly sieved, homogenised soil samples have been analysed, resulting in highly reproducible treatment replicates (Herrmann and Bölscher 2015). Water-amended sieved soil samples usually dissipate heat at a constant rate between 1–10 $\mu W\ g^{-1}$ soil with standard errors in the same magnitude as CO_2 respiration measurements (Herrmann and Bölscher 2015). In the current study, we observed a different pattern, namely that heat dissipation rates in some water amended undisturbed soil samples was of the same order of magnitude as in glucose amended soil samples (see Fig. S1 and S2). When sieving soil samples for preparation according to standard protocols, soil samples are well aerated and POM > 2 mm is mechanically removed. This is not the case for undisturbed soil cores where soil structure is intact and different organic material, such as plant residues, roots and their exudates are therefore available. The saturation and drainage of samples might have resulted in the solubilisation of greater quantities of resources, similar to water extractable organic C measurements when soil samples are leached with deionised water to measure dissolvable organic matter (Surey et al. 2020). This additional mobilising soil C source also likely influenced the measured heat dissipation of the glucose-amended samples; although the effect may have been masked by the readily available added glucose C source. This would explain the high within soil treatment standard errors compared to previously published studies (Herrmann and Bölscher 2015; Yang et al. 2024).

The time required to dissipate 50 % of total heat from undisturbed soil cores after glucose addition was similar to routinely carried out measurements on sieved, homogenised soil samples (Dufour et al. 2022; Yang et al. 2024), indicating that the microbial communities in an intact soil structure had a similar response to the availability of substrate. In all experiments, this rate of heat dissipation was positively correlated to the total energy production, but structural and OM indicators were only able to explain 6 to 50 % of its variance. Only for the experiments with water addition to the pore size range of 15 – 75 μm did the predictive power increase significantly to 63 % when the matrix grey value was taken into account as an additional predictor variable. The lower predictive power of soil structural indicators for heat dissipation rates was also corroborated for mineralisation rates by a previous study based on glucose CO_2 respiration in soil cores taken under contrasting land uses (Schlüter et al. 2022a). Here, further research is required to validate the impact of OM in calorimetric measurements: one possibility would be to use ^{14}C labelled dissolved OC in combination with heat dissipation measurements, and ^{14}C imaging and zymography to characterise biological activity in the tested pore size ranges (Kravchenko et al. 2021).

Overall, the results presented here show that the combination of isothermal calorimetry of undisturbed soil cores with X-ray CT provides new insights into the relation between soil structure and biological activity. The various pore structure indicators and the background porosity explained the majority of the variability in total heat dissipated which could be used to improve modelling of soil OM turnover at different scales (Meurer et al. 2020a; Meurer et al. 2020b; Vogel et al. 2015; Zech et al. 2022). This is particularly true for models that have already taken into account different pore size distributions as an indicator of biological activity and POM-pore distances as an indicator for the physical protection of POM. However, the characterization of the microbial communities, which might have been effected by the different conditions in the field (Furtak et al., 2017), and their relationship with the different soil structures could also have affected the total heat dissipation and the heat dissipation rates. The latter was insufficiently explained by the indicators determined in the experiments with added water. In future studies, characterisation of the microbial communities and their responses to labile OM sources, e.g. glucose solution, could provide additional information on why the different POM and structure indicators could not explain the different heat release rates in all experiments.

5. Conclusion

The study shows that the tested agricultural management practices created significantly different soil structures, all of which provided microbial habitats that enabled microorganisms to mineralise added glucose solution in the two tested pore size ranges of 3 – 75 μm and 15 – 75 μm. It is readily established that different pore size ranges are related to biological activity in undisturbed soils samples. Here, we show that active porosity and pore surface density are key indicators of heat dissipation, particularly in the pore size range of 15 – 75 μm. The grey value of the soil matrix enhances the predictive power of heat dissipation, especially after glucose addition to smaller pores (3 – 15 μm), highlighting the importance of the non-visible pores for biological activity. However, POM volume and occlusion do not significantly explain the variance in heat dissipation.

The study shows that these pore characteristics also determine the biological activity in response to water addition and the subsequent mobilisation of OM within the sample, a process that occurs regularly under natural conditions. The hypothesis that recent rhizosphere C inputs in the maize systems affect heat dissipation in intact soil cores warrants further investigation.

Overall, the study emphasizes the complexity of soil habitats and the need to consider various pore characteristics to understand biological activity in intact soil structures. The quantification of these structural indicators could be used to improve soil OM turnover models under various land management practices. Future research could use the presented procedure to study biological activity in intact soil structures based on isothermal calorimetry. One way would be to focus on higher resolution studies and additional measures to quantify organic matter and its impact on microbial processes.

CRediT authorship contribution statement

Frederic Leuther: Writing – original draft, Visualization, Validation, Methodology, Investigation, Funding acquisition, Formal analysis, Data curation, Conceptualization. **Dorte Fischer:** Writing – review & editing, Visualization, Investigation, Formal analysis, Data curation. **Naoise Nunan:** Writing – review & editing, Supervision, Conceptualization. **Katharina H.E. Meurer:** Writing – review & editing, Methodology. **Anke M. Herrmann:** Writing – review & editing, Supervision, Project administration, Methodology, Funding acquisition, Conceptualization.

Declaration of competing interest

The authors declare that they have no known competing financial interests or personal relationships that could have appeared to influence the work reported in this paper. Naoise Nunan is an Editor-in-Chief for Geoderma and was not involved in the editorial review or the decision to publish this article.

Acknowledgment

We thank the Faculty of Natural Resources and Agricultural Sciences of the Swedish University of Agricultural Science (SLU) for their financial support and the Säby Research Station for access and maintance of to the long-term agricultural field trials (LTE R4-0009).

Funding

This study was funded through an internal SLU starting grant when AMH took on her professorship in Soil Nutrient Cycling. In addition, FL was funded by The Royal Swedish Academy of Agriculture and Forestry (KSLA grant number GFS2022-0122). NN and AMH where funded by the European Unioń s Horizon 2020 research and innovation programme (EJP SOIL, grant number 862695; project EnergyLink), and KHEM received funding from the Swedish Research Council (FORMAS grant number 2022-00307).

Appendix A. Supplementary data

Supplementary data to this article can be found online at https://doi.org/10.1016/j.geoderma.2025.117290.

Data availability

The source data underlying Figs. 1 – 5 and Table 1 – 4 are provided in this paper. Segmented X-ray CT data of the different soil cores will be uploaded at the Soil Structure Library hosted by the Helmholtz-Centre for Environmental Research - UFZ, Germany (https://structurelib.ufz.de/). Additional image data, as well as image analysis codes, are available from the authors upon request.

References

Arellano-Caicedo, C., Ohlsson, P., Bengtsson, M., Beech, J.P., Hammer, E.C., 2021. Habitat geometry in artificial microstructure affects bacterial and fungal growth, interactions, and substrate degradation. In *Commun. Biol.* 4 (1), 1226. https://doi.org/10.1038/s42003-021-02736-4.

Barros Pena, Nieves (2018): Calorimetry and Soil Biodegradation: Experimental Procedures and Thermodynamic Models. In Ederio Dino Bidoia, Renato Nallin Montagnolli (Eds.): Toxicity and Biodegradation Testing. New York, NY: Springer New York, pp. 123–145.

Berg, S., Kutra, D., Kroeger, T., Straehle, C.N., Kausler, B.X., Haubold, C., et al., 2019. ilastik: interactive machine learning for (bio)image analysis. In *Nat. Methods* 16 (12), 1226–1232. https://doi.org/10.1038/s41592-019-0582-9.

Bergkvist, G., Bath, B., Öborn, I., 2011. The design of a new cropping system experiment to be used as a research platform-maize and winter wheat in monoculture and rotations. In *Aspects of Applied Biology* 113, 61–66.

Bhattacharyya, R., Rabbi, S.M.F., Zhang, Y., Young, I.M., Jones, A.R., Dennis, P.G., et al., 2021. Soil organic carbon is significantly associated with the pore geometry, microbial diversity and enzyme activity of the macro-aggregates under different land uses. In *Science of the Total Environment* 778, 146286. https://doi.org/10.1016/j.scitotenv.2021.146286.

Bodner, G., Zeiser, A., Keiblinger, K., Rosinger, C., Winkler, S.K., Stumpp, C., Weninger, T., 2023. Managing the pore system: Regenerating the functional pore spaces of natural soils by soil-health oriented farming systems. Soil Tillage Res. 234, 105862. https://doi.org/10.1016/j.still.2023.105862.

Bronick, C.J., Lal, R., 2005. Soil structure and management: a review. In *Geoderma* 124 (1), 3–22. https://doi.org/10.1016/j.geoderma.2004.03.005.

Da Silva, A.R., Lima, R.P.de, 2015. soilphysics: An R package to determine soil preconsolidation pressure. Comput. Geosci. 84, 54–60. https://doi.org/10.1016/j.cageo.2015.08.008.

Diel, J., Vogel, H.-J., Schlüter, S., 2019. Impact of wetting and drying cycles on soil structure dynamics. In *Geoderma* 345, 63–71. https://doi.org/10.1016/j.geoderma.2019.03.018.

Doran, J.W., Zeiss, M.R., 2000. Soil health and sustainability: managing the biotic component of soil quality. In *Appl. Soil Ecol.* 15 (1), 3–11. https://doi.org/10.1016/S0929-1393(00)00067-6.

Doube, M., Kłosowski, M.M., Arganda-Carreras, I., Cordelières, F.P., Dougherty, R.P., Jackson, J.S., et al., 2010. BoneJ: Free and extensible bone image analysis in ImageJ. In *Bone* 47 (6), 1076–1079. https://doi.org/10.1016/j.bone.2010.08.023.

Dufour, L.J.P., Herrmann, A.M., Leloup, J., Przybylski, C., Foti, L., Abbadie, L., Nunan, N., 2022. Potential energetic return on investment positively correlated with overall soil microbial activity. In *Soil Biology and Biochemistry* 173, 108800. https://doi.org/10.1016/j.soilbio.2022.108800.

Erktan, A., Or, D., Scheu, S., 2020. The physical structure of soil: Determinant and consequence of trophic interactions. In *Soil Biol. Biochem.* 148, 107876. https://doi.org/10.1016/j.soilbio.2020.107876.

Harris, J.A., Ritz, K., Coucheney, E., Grice, S.M., Lerch, T.Z., Pawlett, M., Herrmann, A. M., 2012. The thermodynamic efficiency of soil microbial communities subject to long-term stress is lower than those under conventional input regimes. In *Soil Biol. Biochem.* 47, 149–157. https://doi.org/10.1016/j.soilbio.2011.12.017.

Hartmann, M., Six, J., 2023. Soil structure and microbiome functions in agroecosystems. Nat. Rev. Earth Environ. 4 (1). https://doi.org/10.1038/s43017-022-00366-w.

Hermle, S., Anken, T., Leifeld, J., Weisskopf, P., 2008. The effect of the tillage system on soil organic carbon content under moist, cold-temperate conditions. In *Soil and Tillage Research* 98 (1), 94–105. https://doi.org/10.1016/j.still.2007.10.010.

Herrmann, A.M., Bölscher, T., 2015. Simultaneous screening of microbial energetics and CO2 respiration in soil samples from different ecosystems. In *Soil Biology and Biochemistry* 83, 88–92. https://doi.org/10.1016/j.soilbio.2015.01.020.

Herrmann, A.M., Coucheney, E., Nunan, N., 2014. Isothermal Microcalorimetry Provides New Insight into Terrestrial Carbon Cycling. In *Environmental Science & Technology* 48 (8), 4344–4352. https://doi.org/10.1021/es403941h.

John, B., Yamashita, T., Ludwig, B., Flessa, H., 2005. Storage of organic carbon in aggregate and density fractions of silty soils under different types of land use. In *Geoderma* 128 (1), 63–79. https://doi.org/10.1016/j.geoderma.2004.12.013.

Furtak, K., Gawryjolek, K., Gajda, A.M., Galazka, A., 2017. Effects of maize and winter wheat grown under different cultivation techniques on biological activity of soil. Plant, Soil and Environment 63 (10), 449–454. https://doi.org/10.17221/486/2017-PSE.

Kassambara, A. (2020): rstatix: pipe-friendly framework for basic statistical tests.

Keiluweit, M., Nico, P.S., Kleber, M., Fendorf, S., 2016. Are oxygen limitations under recognized regulators of organic carbon turnover in upland soils? In *Biogeochemistry* 127 (2), 157–171. https://doi.org/10.1007/s10533-015-0180-6.

Keiluweit, M., Wanzek, T., Kleber, M., Nico, P., Fendorf, S., 2017. Anaerobic microsites have an unaccounted role in soil carbon stabilization. In *Nat. Commun.* 8 (1), 1–10. https://doi.org/10.1038/s41467-017-01406-6.

Klöffel, T., Larsbo, M., Jarvis, N., Barron, J., 2024. Freeze-thaw effects on pore space and hydraulic properties of compacted soil and potential consequences with climate change. In *Soil and Tillage Research* 239, 106041. https://doi.org/10.1016/j.still.2024.106041.

Kravchenko, A., Guber, A., Gunina, A., Dippold, M., Kuzyakov, Y., 2021. Pore-scale view of microbial turnover: Combining C imaging, μCT and zymography after adding soluble carbon to soil pores of specific sizes. In *Eur. J. Soil. Sci.* 72 (2), 593–607. https://doi.org/10.1111/ejss.13001.

Kravchenko, A.N., Guber, A.K., Razavi, B.S., Koestel, J., Quigley, M.Y., Robertson, G.P., Kuzyakov, Y., 2019. Microbial spatial footprint as a driver of soil carbon stabilization. In *Nat. Commun.* 10 (1), 1–10. https://doi.org/10.1038/s41467-019-11057-4.

Kuzyakov, Y., Blagodatskaya, E., 2015. Microbial hotspots and hot moments in soil: Concept & review. In *Soil Biol. Biochem.* 83, 184–199. https://doi.org/10.1016/j.soilbio.2015.01.025.

Legland, D., Arganda-Carreras, I., Andrey, P., 2016. MorphoLibJ: integrated library and plugins for mathematical morphology with ImageJ. In *Bioinformatics* 32 (22), 3532–3534. https://doi.org/10.1093/bioinformatics/btw413.

Lehmann, J., Hansel, C.M., Kaiser, C., Kleber, M., Maher, K., Manzoni, S., et al., 2020. Persistence of soil organic carbon caused by functional complexity. In *Nat. Geosci.* 13 (8), 529–534. https://doi.org/10.1038/s41561-020-0612-3.

Leuther, F., Mikutta, R., Wolff, M., Kaiser, K., Schlüter, S., 2023. Structure turnover times of grassland soils under different moisture regimes. In *Geoderma* 433, 116464. https://doi.org/10.1016/j.geoderma.2023.116464.

Leuther, F., Schlüter, S., 2021. Impact of freeze–thaw cycles on soil structure and soil hydraulic properties. In *Soil* 7 (1), 179–191. https://doi.org/10.5194/soil-7-179-2021.

Leuther, F., Wolff, M., Kaiser, K., Schumann, L., Merbach, I., Mikutta, R., Schlüter, S., 2022. Response of subsoil organic matter contents and physical properties to long-term, high-rate farmyard manure application. In *Eur. J. Soil. Sci.* 73 (2), e13233. https://doi.org/10.1111/ejss.13233.

Longepierre, M., Widmer, F., Keller, T., Weisskopf, P., Colombi, T., Six, J., Hartmann, M., 2021. Limited resilience of the soil microbiome to mechanical compaction within four growing seasons of agricultural management. In *ISME Communications* 1 (1), 44. https://doi.org/10.1038/s43705-021-00046-8.

Lucas, M., Schlüter, S., Vogel, H.-J., Vetterlein, D., 2019. Soil structure formation along an agricultural chronosequence. In *Geoderma* 350, 61–72. https://doi.org/10.1016/j.geoderma.2019.04.041.

Mendiburu, Felipe de; Yaseen, Muhammad (2020): agricolae: Statistical Procedures for Agricultural Research (R Package, Version).

Meurer, K.H.E., Barron, J., Chenu, C., Coucheney, E., Fielding, M., Hallett, P., et al., 2020a. A framework for modelling soil structure dynamics induced by biological activity. In *Glob. Chang. Biol.* 26 (10), 5382–5403. https://doi.org/10.1111/gcb.15289.

Meurer, K.H.E., Chenu, C., Coucheney, E., Herrmann, A.M., Keller, T., Kätterer, T., et al., 2020b. Modelling dynamic interactions between soil structure and the storage and turnover of soil organic matter. In *Biogeosciences* 17 (20), 5025–5042. https://doi.org/10.5194/bg-17-5025-2020.

Mevik, B.-H., Wehrens, R., 2007. The pls Package: Principal Component and Partial Least Squares Regression in R. In *J. Stat. Soft.* 18 (2), 1–23. https://doi.org/10.18637/jss.v018.i02.

Munkholm, L.J., Hansen, E.M., Olesen, J.E., 2008. The effect of tillage intensity on soil structure and winter wheat root/shoot growth. In *Soil Use Manag.* 24 (4), 392–400. https://doi.org/10.1111/j.1475-2743.2008.00179.x.

Munkholm, L.J., Heck, R.J., Deen, B., 2013. Long-term rotation and tillage effects on soil structure and crop yield. In *Soil and Tillage Research* 127, 85–91. https://doi.org/10.1016/j.still.2012.02.007.

Nunan, N., Leloup, J., Ruamps, L.S., Pouteau, V., Chenu, C., 2017. Effects of habitat constraints on soil microbial community function. In *Sci. Rep.* 7 (1), 4280. https://doi.org/10.1038/s41598-017-04485-z.

Ortega-Ramírez, Patricia; Pot, Valérie; Laville, Patricia; Schlüter, Steffen; Amor-Quiroz, David Arturo; Hadjar, Dalila et al. (2023): Pore distances of particulate organic matter predict N2O emissions from intact soil at moist conditions. In *Geoderma* 429, p. 116224. DOI: 10.1016/j.geoderma.2022.116224.

R Core Team, 2020. R: A language and environment for statistical computing. R Foundation for Statistical Computing, Vienna, Austria.

Rabbi, S.M.F., Daniel, H., Lockwood, P.V., Macdonald, C., Pereg, L., Tighe, M., et al., 2016. Physical soil architectural traits are functionally linked to carbon decomposition and bacterial diversity. In *Sci. Rep.* 6 (1), 33012. https://doi.org/10.1038/srep33012.

Rabot, E., Wiesmeier, M., Schlüter, S., Vogel, H.-J., 2018. Soil structure as an indicator of soil functions: a review. In *Geoderma* 314, 122–137. https://doi.org/10.1016/j.geoderma.2017.11.009.

Renard, P., Allard, D., 2013. Connectivity metrics for subsurface flow and transport. In *Advances in Water Resources* 51, 168–196. https://doi.org/10.1016/j.advwatres.2011.12.001.

Schindelin, J., Arganda-Carreras, I., Frise, E., Kaynig, V., Longair, M., Pietzsch, T., et al., 2012. Fiji: an open-source platform for biological-image analysis. In *Nature Methods* 9 (7), 676–682. https://doi.org/10.1038/nmeth.2019.

Schlüter, S., Roussety, T., Rohe, L., Guliyev, V., Blagodatskaya, E., Reitz, T., 2022a. Land use impact on carbon mineralization in well aerated soils is mainly explained by variations of particulate organic matter rather than of soil structure. In *Soil* 8 (1), 253–267. https://doi.org/10.5194/soil-8-253-2022.

Schlüter, S., Großmann, C., Diel, J., Wu, G.-M., Tischer, S., Deubel, A., Rücknagel, J., 2018. Long-term effects of conventional and reduced tillage on soil structure, soil ecological and soil hydraulic properties. In *Geoderma* 332, 10–19. https://doi.org/10.1016/j.geoderma.2018.07.001.

Schlüter, S., Leuther, F., Albrecht, L., Hoeschen, C., Kilian, R., Surey, R., et al., 2022b. Microscale carbon distribution around pores and particulate organic matter varies with soil moisture regime. In *Nat. Commun.* 13 (1), 2098. https://doi.org/10.1038/s41467-022-29605-w.

Shi, A., Chakrawal, A., Manzoni, S., Fischer, B.M.C., Nunan, N., Herrmann, A.M., 2021. Substrate spatial heterogeneity reduces soil microbial activity. In *Soil Biol. Biochem.* 152, 108068. https://doi.org/10.1016/j.soilbio.2020.108068.

Surey, R., Lippold, E., Heilek, S., Sauheitl, L., Henjes, S., Horn, M.A., et al., 2020. Differences in labile soil organic matter explain potential denitrification and denitrifying communities in a long-term fertilization experiment. In *Appl. Soil Ecol.* 153, 103630. https://doi.org/10.1016/j.apsoil.2020.103630.

van Genuchten, M.T., 1980. A Closed-form Equation for Predicting the Hydraulic Conductivity of Unsaturated Soils. In *Soil Sci. Soc. Am. J.* 44 (5), 892–898. https://doi.org/10.2136/sssaj1980.03615995004400050002x.

Vogel, H.J., Weller, U., Schlüter, S., 2010. Quantification of soil structure based on Minkowski functions. In *Comput. Geosci.* 36 (10), 1236–1245. https://doi.org/10.1016/j.cageo.2010.03.007.

Vogel, L.E., Makowski, D., Garnier, P., Vieublé-Gonod, L., Coquet, Y., Raynaud, X., et al., 2015. Modeling the effect of soil meso- and macropores topology on the biodegradation of a soluble carbon substrate. In *Advances in Water Resources* 83, 123–136. https://doi.org/10.1016/j.advwatres.2015.05.020.

Weller, U., Albrecht, L., Schlüter, S., Vogel, H.J., 2022. An open Soil Structure Library based on X-ray CT data. In *Soil* 8 (2), 507–515. https://doi.org/10.5194/soil-8-507-2022.

Wickham, Hadley (2016): ggplot2: elegant graphics for data analysis. 2nd ed.: Springer Cham.

Wickham, H., Averick, M., Bryan, J., Chang, W., McGowan, L.D., François, R., et al., 2019. Welcome to the Tidyverse. J. Open Source Softw. 4 (43), 1686. https://doi.org/10.21105/joss.01686.

Yang, S., Di Lodovico, E., Rupp, A., Harms, H., Fricke, C., Miltner, A., et al., 2024. Enhancing insights: exploring the information content of calorespirometric ratio in dynamic soil microbial growth processes through calorimetry. Front. Microbiol. 15, 1321059. https://doi.org/10.3389/fmicb.2024.1321059.

Young, I.M., Crawford, J.W., Nunan, N., Otten, W., Spiers, A., 2008. Microbial distribution in soils: physics and scaling. In *Adv. Agron.* 100, 81–121.

Zech, S., Schweizer, S.A., Bucka, F.B., Ray, N., Kögel-Knabner, I., Prechtel, A., 2022. Explicit spatial modeling at the pore scale unravels the interplay of soil organic carbon storage and structure dynamics. In *Glob. Chang. Biol.* 28 (15), 4589–4604. https://doi.org/10.1111/gcb.16230.

Zuber, S.M., Villamil, M.B., 2016. Meta-analysis approach to assess effect of tillage on microbial biomass and enzyme activities. In *Soil Biol. Biochem.* 97, 176–187. https://doi.org/10.1016/j.soilbio.2016.03.011.